British Journal of Pharmacology (2002) 135, 581–588 © 2002 Nature Publishing Group All rights reserved 0007–1188/02 $25.00

www.nature.com/bjp

Intracellular distribution of peroxynitrite during doxorubicin cardiomyopathy: evidence for selective impairment of myofibrillar creatine kinase

[1]Michael J. Mihm, [1]Fushun Yu, [1]David M. Weinstein, [2]Peter J. Reiser & *,[1]John Anthony Bauer

[1]Division of Pharmacology,College of Pharmacy and OSU Heart & Lung Research Institute, Columbus, Ohio, U.S.A. and [2]College of Dentistry, Ohio State University, Columbus, OH 43210, U.S.A.

Cardiac peroxynitrite and protein nitration are increased during doxorubicin cardiotoxicity, but the intracellular targets and functional consequences have not been defined. We investigated the intracellular distribution of protein nitration during doxorubicin cardiotoxicity in mice. Following *in vivo* cardiac function assessments by echocardiography, cardiac tissues were prepared for immunohistochemistry and electron microscopy 5 days after doxorubicin (20 mg kg^{-1}) or vehicle control. Increased cardiac 3-nitrotyrosine was observed using light microscopy in doxorubicin treated animals. Immunogold electron microscopy (55,000×) revealed increased myofibrillar and mitochondrial 3-nitrotyrosine levels following doxorubicin, but cellular 3-nitrotyrosine density was 2 fold higher in myofibrils. We therefore investigated the actions of peroxynitrite on intact cardiac contractile apparatus. Skinned ventricular trabeculae were exposed to physiologically relevant peroxynitrite concentrations (50 or 300 nM) for 1 h, then Ca^{2+} induced contractile responses were measured in the presence of ATP (4 mM) or phosphocreatine (12 mM) as high energy phosphate supplier. ATP maximal force generation was unaltered after 50 nM peroxynitrite, but phosphocreatine/ATP response was reduced (0.99 ± 0.63 vs 1.59 ± 0.11), suggesting selective inactivation of myofibrillar creatine kinase (MM-CK). Reduction of ATP maximal force was observed at 300 nM peroxynitrite and phosphocreatine/ATP response was further reduced (0.64 ± 0.30). Western blotting showed concentration dependent nitration of MM-CK in treated trabeculae. Similarly, cardiac tissues from doxorubicin treated mice demonstrated increased nitration and inactivation of MM-CK compared to controls. These results demonstrate that peroxynitrite-related protein nitration are mechanistic events in doxorubicin cardiomyopathy and that the cardiac myofibril is an important oxidative target in this setting. Furthermore, MM-CK may be a uniquely vulnerable target to peroxynitrite *in vivo*.
British Journal of Pharmacology (2002) **135,** 581–588

Keywords: Doxorubicin; peroxynitrite; myofibrillar creatine kinase; nitric oxide; cardiac; echocardiography; 3-nitrotyrosine; nitration; cardiomyopathy; electron micropscopy

Abbreviations: 3NT, 3-nitro-L-tyrosine; CO, cardiac output; DOX, doxorubicin; FS, fractional shortening; LV, left ventricular; LVIDd, left ventricular internal dimension at diastole; LVIDs, left ventricular internal dimension at systole; M-CK, myofibrillar creatine kinase (monomer); MM-CK, myofibrillar creatine kinase (dimer); $ONOO^-$, peroxynitrite; VTI, velocity-time integral

Introduction

Doxorubicin (DOX) is an important anticancer drug with a wide array of therapeutic uses (e.g., breast and bladder cancers, Hodgkin's lymphomas, and others) (Hortobagyi, 1997; Blum & Carter, 1974). Despite its frequent use, the clinical utility of DOX is severely compromised by dose-limiting cardiotoxicities (Singal, 1987;Doroshow *et al*., 1979). The general approach to reduce this risk is the implementation of lifetime limits in DOX dosing for cancer patients, but dose-dependencies and timing of DOX toxicity are often variable and difficult to predict (Hortobagyi, 1997; Singal, 1987; Kwok & Richardson, 2000). While many patients exhibit cumulative dose-dependent toxicities, others experience first-dose acute life-threatening reactions, or delayed cardiomyopathies manifesting months to years following cessation of therapy (Hortobagyi, 1997; Singal, 1987; Kwok & Richardson, 2000). An important recent study also demonstrated that mortality is very high in DOX-related cardiomyopathy (50% mortality within 2 years of diagnosis), and is distinct relative to other forms of cardiac disease (Felker *et al*., 2000). Thus, while DOX cardiotoxicity has been known for many years, it remains a contemporary problem (Swain, 1999; Lipshultz & Grenier, 1999; Muggia & Speyer, 1999)

Increased reactive oxygen species formation and resultant oxidative cardiomyocyte injury have been implicated as mechanisms of DOX cardiotoxicity, particularly increased superoxide anion formation (Yen *et al*., 1996; Hasinoff *et al*., 1998). We have recently demonstrated that peroxynitrite ($ONOO^-$) is formed in cardiac myocytes during DOX cardiotoxicity in mice (Weinstein *et al*., 2000). Peroxynitrite is a highly cytotoxic oxidant formed in the nearly instantaneous reaction of nitric oxide with superoxide anion (Radi *et al*., 1991). $ONOO^-$ can participate in a variety of oxidative chemistries, and relative to other biological

*Author for correspondence at: 412 Riffe Building, 500 West 12th Avenue, Columbus, Ohio 43210-1291, U.S.A.;
E-mail: bauer.140@osu.edu

oxidants, avidly causes nitration of tyrosine residues, resulting in post-translational modification of protein-bound tyrosine to 3-nitrotyrosine (3NT) (Beckman & Koppenol, 1996). We and others have demonstrated that protein nitration is a relevant phenomenon in multiple settings of decompensated cardiac failure (Weinstein *et al*., 2000; Kooy *et al*., 1997). Although protein nitration has been demonstrated to mediate some of the toxic effects of ONOO$^-$ *in vitro*, including enzyme inhibition, the putative cellular targets and biochemistries of ONOO$^-$ *in vivo* are only beginning to be investigated (Ischiropoulos, 1998).

We have demonstrated extensive cardiac protein nitration during DOX cardiotoxicity, and found that extent of protein nitration was statistically correlated to cardiac dysfunction, implicating ONOO$^-$ and attendant protein nitration as important mediators of some aspects of DOX-induced cardiac failure (Weinstein *et al*., 2000). Much clinical and experimental evidence suggests that cardiomyocyte mitochondria are important intracellular targets of reactive oxygen species during DOX cardiotoxicity (Gille & Nohl, 1997; Papadopoulou *et al*., 1999). The putative intracellular organelles associated with ONOO$^-$-mediated protein nitration are incompletely defined; however, we have demonstrated that protein nitration of cardiac myofibrils, the protein structure that mediates myocyte contraction, is significantly elevated during DOX cardiotoxicity (Weinstein *et al*., 2000). Here we employed high-magnification electron microscopy to test the hypothesis that cardiac myofibrils are a predominant and important intracellular target of ONOO$^-$ during DOX cardiotoxicity. We then investigated mechanistic aspects and functional consequences of nanomolar ONOO$^-$ exposure and attendant protein nitration to the intact myofibrillar contractile structure, with particular attention to the oxidant sensitive energetic controller, myofibrillar creatine kinase.

Methods

Animals

Male, CF-1 mice (Harlan, Indianapolis, IN, U.S.A.) weighing 28–32 g were administered a single dose of doxorubicin HCl (Bedford laboratories, Bedford, OH, U.S.A.) 20 mg kg^{-1}, i.p., and studied 5 days afterwards. This time point was chosen as >five final half-lives of elimination of DOX from both plasma and cardiac tissue in mice (van der Vijgh *et al*., 1990). All animal studies have been carried out in accordance with the Declaration of Helsinki and/or with the Guide for the Care and Use of Laboratory Animals as adopted and promulgated by the U.S. National Institutes of Health.

Murine echocardiography

Five days following DOX administration, *in vivo* cardiovascular function was determined using a Sonos 5500 echocardiography unit (Hewlett-Packard, Andover, MA, U.S.A.), as previously described (Weinstein *et al*., 2000). Mice ($n=6-8$ per treatment group) were anaesthetized by halothane inhalation (~1% halothane in 95/5% oxygen/CO_2). Normothermia was maintained by heating pad. A 15 MHz pediatric probe placed in the parasternal, short axis orientation recorded LV systolic and diastolic internal dimensions. Three loops of M-mode data were captured for each animal, and data were averaged from at least five beat cycles per loop. Parameters were determined using the American Society for Echocardiography leading-edge technique in blinded fashion. These parameters allowed the determination of LV fractional shortening (FS) by the equation: $FS=[(LVIDd-LVIDs)/LVIDd]\times 100\%$, where LVID refers to the LV internal dimension at diastole (d) and systole (s). Ascending aortic flow waveforms were recorded using a continuous wave Doppler flow probe oriented in a short axis, suprasternal manner. Velocity-time integrals (VTI) were calculated from these waveforms. After sacrifice, aortic root cross-sectional area was measured and cardiac output was calculated by the equation: CO = Heart rate × VTI × aortic cross-sectional area.

Cardiac immunohistochemistry

Mice ($n=6-8$ per treatment group) were sacrificed with 100 mg kg^{-1} i.p. pentobarbital sodium (Abbott Laboratories, Chicago, IL, U.S.A.). The apical portion of the heart was bisected just distal to the mitral valve and immersed in 10% formalin. Tissues were paraffin embedded and blocked according to standard procedures. Five micron sections were immunostained using polyclonal primary antibodies for 3-nitrotyrosine (anti-3-NT, Upstate Biotechnology, Lake Placid, NY, U.S.A; 1 : 400) as previously described (Mihm *et al*., 1999). Exposure of the tissue sections to 0.06% w v^{-1} diaminobenzidine followed by hematoxylin counterstaining provided visualization of immunoreactivity. Serial tissue sections from DOX treated animals were used to validate antibody specificity for 3-NT (antibody pre-adsorbed with 5 mM free 3-NT) as staining controls.

Left ventricular images were captured using a digital camera (Polaroid, Cambridge, MA, U.S.A.) and transferred into research-based digital image analysis software (Image Pro Plus, Media Cybernetics, Silver Spring, MD, U.S.A.). Extent of immunoreactivity in the LV was determined in the tissues by applying intensity thresholding analysis, as previously described (Mihm *et al*., 1999). A criterion for thresholding was set such that less than 2% of the total pixels representing a control (non-immunoreactive) tissue fell in the gray-scale pixel intensity range of 0–155. Therefore, the percentage of total LV image pixels in the 0–155 range was used as a semi-quantitative measure of relative immunoreactivity.

Electron microscopy and immunocytochemistry

Cardiac left ventricular tissue samples ($n=6-8$ per treatment group) were obtained for electron microscopic immunocytochemistry from CTRL and DOX animals following echocardiographic assessment on day 5, as we have previously described (Crouser *et al*., 2000). Left ventricular free wall was excised and immersed in isotonic fixative (4% paraformaldhyde, 0.5% glutaraldehyde, in 0.1 M phosphate buffer, pH 7.4, with 0.1 M sucrose). Tissues were minced such that longitudinal sections were readily obtained, and incubated for 1 h at room temperature, followed by overnight fixation at 4°C. The following morning, tissues were dehydrated through an ascending series of ethanol solutions. Tissues were then infiltrated with and embedded in LR white

resin. Thin sections (80–90 nm) were cut on a Reichart Ultracut E microtome and mounted on Formvar coated nickel grids.

In preparation for immunocytochemistry, grids were blocked (1% BSA, 0.1 M glycine in PBS) for 1 h, then incubated for 2 h with rabbit polyclonal antibody raised against 3NT (anti-3NT, 1 : 500, Upstate Biotechnology, Lake Placid, NY, U.S.A.). Staining (isotypic) control tissues were exposed for the same duration to nonimmune rabbit IgG (1 : 200; Vector Labs) in place of primary antibody. Following a series of washes, grids were incubated for 1 h with 10 nm Immunogold-linked, EM grade, goat anti-rabbit IgG (1 : 20 dilution, Electron Microscopy Sciences, Fort Washington, PA, U.S.A.). Following another series of washes, grids were successively immersed in 2% glutaraldehyde, 0.5% osmium tetroxide, then stained with 2% uranyl acetate and lead citrate before visualization with a Phillips CM 12 tunneling electron microscope. Preliminary experiments were conducted to verify the specificity of immunostaining in our laboratory. Pre-incubation of primary antibody with 5 mM free 3NT quenched positive tissue staining, whereas 5 mM TYR had no effect.

Electron micrographs (42,500–55,000× original magnification) were scanned using a Hewlett Packard Scanjet 6200c capable of 1290 × 960 resolution (Palo Alto, CA, U.S.A.) and transferred into research-based digital image analysis software (Image Pro Plus, Media Cybernetics, Silver Spring, MD, U.S.A.) for analysis. Images were calibrated, myofibrillar and mitochondrial structures were defined, and gold particles were segmented for grayscale intensity and gated based on size, then counted and normalized as a function of area and total myocyte area. Intra-observer and inter-observer variability ($n = 10$ myofibrillar and mitochodrial areas, two observers) were each less than 2%.

In vitro *exposure of left ventricular trabeculae to authentic peroxynitrite*

Cardiac trabeculae were exposed to infusions of $ONOO^-$, and assessed for resultant contractile function. Single cardiac trabeculae were isolated as previously described and then suspended in rapidly stirring relaxing solution (Wattanapermpool & Reiser, 1999). $ONOO^-$ was purchased from Upstate Biotechnology (Lake Placid, NY, U.S.A.) and diluted in 0.3 M NaOH in ultrapure water. Immediately before addition, $ONOO^-$ concentrations were confirmed by spectroscopy ($\varepsilon_{302} = 1.62\ mM^{-1}\ cm^{-1}$) (Sampson *et al*., 1996). The half-life of $ONOO^-$ in 0.3 M NaOH was experimentally determined to be 3.3 h. Total $ONOO^-$ doses of 125 and 750 nmoles were infused as 2% volume additions by infusion pump (Harvard Apparatus, Holliston, MA, U.S.A.) for 1 h, achieving steady state $ONOO^-$ concentrations of 50–300 nM (based on $t_{1/2,\ ONOO} = 1$ s at pH 6.8) (Sampson *et al*., 1996).

Three controls were used for ONOO treatment: No addition control, $ONOO^-$ background electrolyte control (0.3 M NaOH), and degraded $ONOO^-$ control (300 nM $ONOO^-$ titrated to pH 6.8 and degraded for 30 min). In all experiments, functional parameters derived from all three control treatments were not statistically different; therefore, these treatments were pooled as one control for further statistical comparisons.

Isolated trabecula force generation

Following $ONOO^-$ administration, trabeculae were mounted between the arms of a direct-current torque motor (Model 300H; Cambridge Technology, Cambridge, MA, U.S.A.) and an isometric tension transducer (Model 403, Cambridge Technology) in an experimental chamber containing relaxing solution. Sarcomere length was assessed by Polaroid camera; the width and depth of trabeculae used in this study were 50–180 μm. Fibre cross-sectional area (CSA) was calculated from the depth and width measurements by assuming an elliptical fibre circumference, as previously described (Wattanapermpool & Reiser, 1999).

Trabecular maximal force generation and calcium sensitivity were assessed as previously described (Wattanapermpool & Reiser, 1999). Two activating solutions were utilized in random sequence, with ATP versus PCr as the primary high energy phosphate supplier. The level of calcium-activated force was measured in ATP solution (as described in Wattanapermpool & Reiser (1999), with the following modifications: 4.4 mM ATP, 12.5 mM PCr, 2 μM ADP) to assess force generation during and subsequent to myosin ATPase mediated energy utilization. Calcium activated force was also measured in PCr solution (0 mM ATP, 12.5 mM PCr, 250 μM ADP) to assess myofibrillar creatine kinase activity *in situ*. No significant differences were detected in control measurements of maximal force generation or calcium sensitivity between these two solutions. All mechanical measurements were performed at 15°C. The peak isometric tension generated was measured in randomized activating solutions ranging from pCa 7.0 to 4.0 at pH 7.0. The maximally activated tension of the trabecula, obtained in the solution with pCa 4.0, was referred to as P_o. Maximal activations were performed after every two consecutive submaximal activations. The measurements on a given fibre were terminated if P_o decreased by 9% or more of the original P_o.

Western blotting

Whole cardiac trabeculae were solublized in gel sample buffer following functional analyses, then loaded onto 10% polyacrylamide gels (1.5 mm). Proteins were electrophoresed under reducing conditions prior to transfer to nitrocellulose membranes. Protein load was verified by silver stain (Sigma Chemical, St. Louis, MO, U.S.A.). Migration of M-CK was confirmed with an antibody against M-CK (anti M-CK, 1:200, Fitzgerald Industries, Concord, MA, U.S.A.). Membranes were immunostained with anti-3NT antibody (1 : 400) as previously described (Mihm *et al*., 2001a).

Creatine kinase activity

CK activity was determined spectrophotometrically by indirectly monitoring ATP formation; the rate of change of absorbance was directly proportional to CK activity, as previously described (Mihm *et al*., 2001a). Myofibrillar fractions were added to the reaction mixture at 25°C, then various concentrations of PCr (0.1–100 mM) were added to start the reaction. Change in absorbance was monitored for 6 min and reflected CK velocity. Each treatment group was investigated at each concentration in triplicate. In preliminary

experiments, ATP formation was demonstrated to be rate-limiting at all CK concentrations analysed by varying CK concentration from 2.5 mg ml^{-1} to 5 g ml^{-1}.

Data handling

Significant differences between treatments were determined using two-tailed Student's *t*-tests or One-way analyses of variance, with *post-hoc* Newman-Keuls tests to evaluate significant comparisons. MM-CK velocity data were fit by Michaelis-Menton kinetics, yielding V_{max} and K_m parameters, using GraphPad Prism software. $P<0.05$ described statistical significance.

Results

Shown in Table 1 are echocardiographic cardiac performance indicators from CTRL and DOX treated mice, 5 days post-treatment. DOX-treated mice exhibited significant decreases in multiple indicators of cardiac performance. LV fractional shortening, maximal aortic velocity, velocity-time integral, and cardiac output were all statistically reduced in DOX treated animals compared to CTRL, in the absence of significant LV dilation (LV inner dimension at systole, diastole).

Shown in Figure 1A are representative photomicrographs from cardiac left ventricles of CTRL and DOX-treated mice (400×). 3NT prevalence was strikingly increased in cardiac myocytes of DOX treated animals versus controls. Staining was predominantly restricted within cardiac myocytes themselves, widespread throughout the myocardium, and not confined to focal immune cell infiltration. Digital image analysis demonstrated a statistically significant increase in 3NT positive staining in DOX treated mice compared to controls (far right panel $P<0.05$).

Shown in Figure 1B,C are representative electron micrographs from the cardiac left ventricles of CTRL and DOX-treated mice. Although the fixation methods used were optimized for antigenicity (4% paraformaldhyde, 0.5% glutaraldehyde), myofibrillar and mitochondrial organelles can be clearly delineated. DOX treatment resulted in the loss of myofibrillar thickness and alignment compared to CTRL (Figure 1B). Figure 1C illustrates the relative distribution of immunogold 3NT staining in CTRL versus DOX treatment and in cardiac myofibrillar versus mitochondrial organelles.

Table 1 Various haemodynamic parameters from *in vivo* echocardiography

	CTRL ($n=6-8$)	*DOX* ($n=6-8$)
M-Mode		
End-diastolic Dimension (cm)	0.34±0.02	0.29±0.03
End-systolic Dimension (cm)	0.19±0.02	0.21±0.02
Fractional Shortening (per cent)	43.2±1.1	27.4±2.0*
Continuous-wave Doppler		
Maximal Aortic Velocity (cm s^{-1})	87.1±3.3	55.4±3.6*
Velocity-Time Intergal (cm)	3.68±0.03	2.50±0.25*
Cardiac Output (ml min^{-1})	14.5±1.2	7.6±1.5*
Heart Rate (b.p.m.)	500±34	374±33*

Parameters reported as means±s.e.mean; *, significant difference from vehicle control, $P<0.05$

Black electron dense circles (10 nm gold particles) represent positively stained tissue. In CTRL images, relatively sparse immunostaining was observed, with roughly equal staining density between myofibrillar and mitochondrial compartments (Figure 1C, top). Staining density was increased in both myofibrillar and mitochondrial spaces in cardiac tissue from DOX treated mice (Figure 1C, middle). A representative image from the preadsorbed staining control (primary antibody preincubated with 5 mM 3NT, see Methods) is shown in Figure 1C, lower panel, demonstrating high antibody specificity for this method.

The quantitative results of digital image analysis of cardiac 3NT immunogold immunocytochemistry in CTRL and DOX treated mice are shown in Figure 2. Using these automated digital imaging methods, approximately 8500 gold particles were counted from electron photomicrographs. Appreciable staining was detected in CTRL tissues in both myofibrillar and mitochondrial spaces, with equivalent 3NT density per myocyte area (Figure 2A). DOX treatment resulted in statistically significant increases in both myofibrillar and mitochondrial 3NT formation compared to CTRL. Myofibrillar tyrosine nitration was elevated 68% in DOX compared to CTRL per square micron; mitochondrial tyrosine nitration was elevated 46%. No significant differences in 3NT density (per area) were detected between myofibrils and mitochondria in the DOX treatment group.

3NT staining was integrated and expressed per cardiac myocyte. Myofibrillar and mitochondrial staining in CTRL tissues were again not statistically different, and DOX treatment again resulted in highly significant increases in 3NT density in both organelles (Figure 2B). However, total nitration load was significantly higher ($P<0.05$) in cardiac myofibrils versus mitochondria, elevated 67% per cardiac myocyte, based on conversions from total cardiomyocyte area measurements (Zhou & Kang, 2000).

Based on our finding that the myofibrillar structure was a predominant site of nitration *in vivo*, we investigated the effects of authentic peroxynitrite on isolated cardiac trabeculae (Figure 3). Trabeculae were exposed to infusions of ONOO$^-$, resulting in sub-micromolar (50–300 nM) steady state concentrations of ONOO$^-$. Calcium activated contractile function and tyrosine nitration were then investigated in isolated trabeculae by established protocols. Average pCa/tension relationships for trabeculae exposed to increasing ONOO$^-$ concentrations are shown in Figure 3A. ONOO$^-$ resulted in concentration-dependent decreases in trabecular maximal force generation, with significant decreases at ONOO$^-$ concentrations as low as 300 nM, when either ATP or phosphocreatine (PCr) was utilized as the primary high energy phosphate supplier (Figure 3B). Steady state concentrations as low as 50 nM ONOO$^-$ resulted in statistically significant decreases in the ratio of PCr/ATP developed force. These results are indicative of selective impairment of myofibrillar creatine kinase (Ventura-Clapier *et al*., 1994). Trabecular content of M-CK (monomer by Western blotting) was unchanged in these groups, however myofibrillar creatine kinase demonstrated concentration-dependent increases in extent of tyrosine nitration when observed by western blot analyses (Figure 3C).

Based on evidence of selective MM-CK impairment in the trabecular peroxynitrite studies, left ventricular myofibrillar creatine kinase activity and nitration were evaluated in DOX

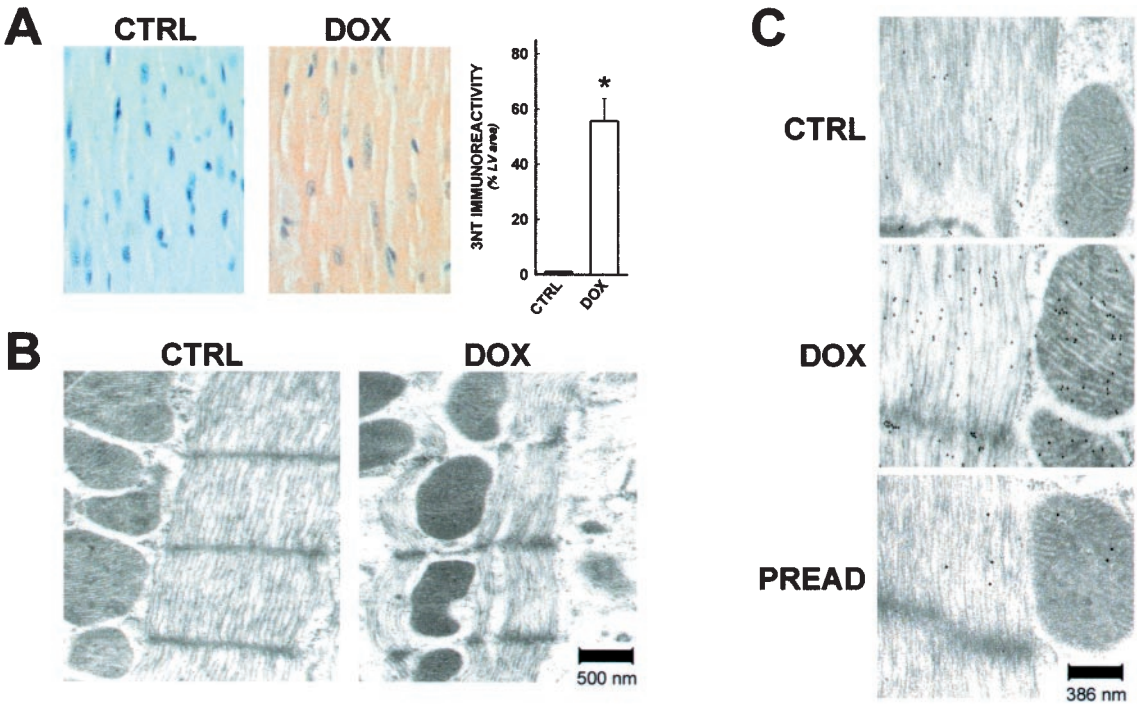

Figure 1 DOX cardiotoxicity is associated with increased cardiac protein nitration. (A) Representative photomicrographs of cardiac left ventricular sections from vehicle control and DOX treated mice probed for 3NT. Brown staining indicates 3NT immunoprevalence. Relative 3NT immunoprevalence expressed as percentage of total left ventricular area analysed demonstrating positive immunoreactivity for 3NT, as determined by digital image analysis (right panel). (B) Immunogold electron microscopy for 3NT was conducted in left ventricular tissue from DOX and CTRL treated mice. Electron dense circles indicate positive staining for 3NT. Left panel: Longitudinal section of left ventricular tissue from vehicle treated control mouse. Cardiac mitochondria observed as circles on left, myofibril observed as striated structure on right (42,500× original magnification). Right panel: Longitudinal LV section from DOX treated mouse demonstrates myofibrillar thinning and irregular striation patterns (42,500× original magnification). (C) Top panel: Representative CTRL image illustrating sparse gold particle density in both myofibrillar and mitochondrial spaces (55,000× original magnification). Middle panel: Representative DOX image demonstrating high gold particle density in both myofibrillar and mitochondrial spaces (55,000× original magnification). Lower panel: Representative preadsorbed staining control (primary antibody preincubated with 5 mM 3NT, see Methods) image from DOX treated mouse (55,000× original magnification). $^*P<0.05$.

treated and CTRL mice. Similar to our *in vitro* findings, DOX treatment *in vivo* resulted in a statistically significant decrease in myofibrillar creatine kinase activity compared to vehicle control (Figure 4A). Furthermore, while total myofibrillar M-CK content was equivalent between treatment groups, DOX treated mice exhibited significant increases in the extent of 3NT formation in M-CK (Figure 4B).

Discussion

In our previous studies we showed that doxorubicin dosing in mice (20 mg kg^{-1} i.p., same dose as employed herein) caused irreversible contractile deficits, and induction of NOS2 (Weinstein *et al*., 2000). The extent of cardiac protein nitration, but not NOS2 immunoprevalence, was also highly correlated to the LV dysfunction observed in these animals, suggesting that peroxynitrite related events participate in this cardiac pathology. While our studies and others have previously implicated oxidative mechanisms in DOX induced cardiomyopathy, the actual sources and/or putative targets involved have not been identified. Here, we demonstrated severe left ventricular dysfunction in a well-established murine model of DOX cardiotoxicity (mimicking the human pathology) to test the hypothesis that the cardiac myofibrillar compartment is an important site of tyrosine nitration during DOX cardiotoxicity. We then investigated the functional consequences of nanomolar $ONOO^-$ formation and attendant protein nitration on isolated cardiac myofibrillar function.

Using echocardiographic techniques, we non-invasively assessed cardiac performance 5 days after a single dose of DOX. This time point was chosen as >five final half lives of elimination of DOX from both plasma and cardiac tissue in mice (van der Vijgh *et al*., 1990). Therefore, at the time of functional and immunocytochemical assessments, DOX was no longer present in the blood or cardiac tissues. We observed significant reductions in cardiac performance measuring a variety of independent parameters. Cardiac contractility, assessed by fractional shortening and stroke volume measures, was markedly reduced during DOX cardiotoxicity. These changes are consistent with clinical observations, in that significant and sustained contractility deficits were observed following cessation of DOX therapy, suggesting that this murine model appears appropriate for mechanistic evaluations (Doroshow *et al*., 1979).

Cardiac mitochondria have been hypothesized as the primary source of reactive oxygen species formation during DOX cardiotoxicity, and mitochondrial injury is an estab-

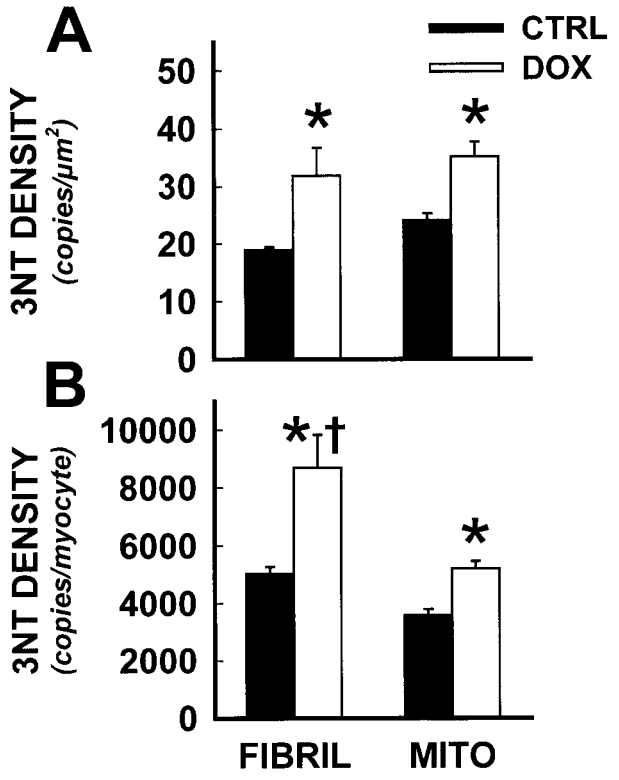

Figure 2 Quantitative image analysis demonstrated high 3NT density in cardiac myofibrils during DOX cardiotoxicity. Quantitative image analysis was conducted on immunogold electron micrographs from CTRL and DOX treated mice. Following area calibrations, myofibrillar and mitochondrial gold particle density was expressed as a function of area (A) and total myocyte area (B). *Statistically significant difference from CTRL, $P<0.05$; †, DOX myofibrillar 3NT density significantly different from DOX mitochondrial staining, $P<0.05$.

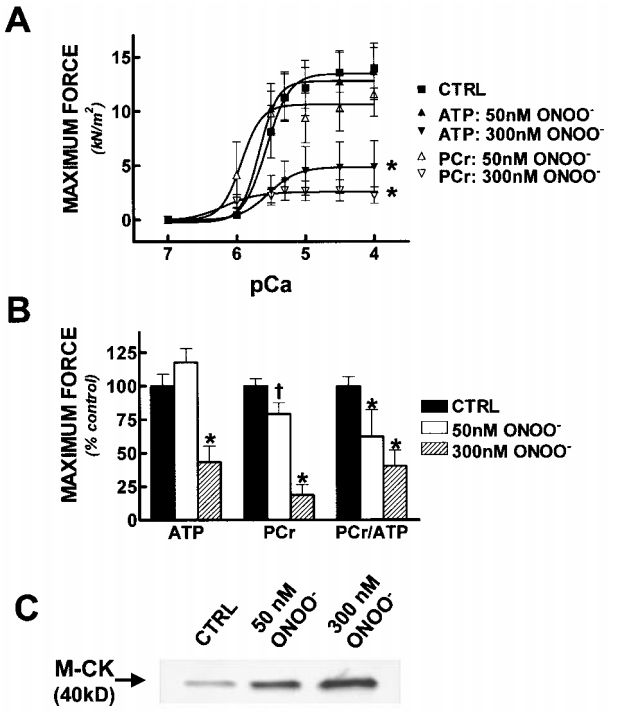

Figure 3 Peroxynitrite inhibited myofibrillar force development and *in situ* creatine kinase activity *in vitro*. Isolated cardiac trabeculae were infused with sub-micromolar concentrations of $ONOO^-$, then ability to generate calcium-activated force and tyrosine nitration were assessed and tyrosine nitration. ATP solutions directly stimulate contractile activity; phosphocreatine (PCr) solutions require active MM-CK to elicit contraction. (A) Average fitted pCa/tension relationships for ATP and PCr solutions following $ONOO^-$ treatment. Control curves for ATP and PCr solutions were not statistically different, and were therefore pooled into one control treatment. (B) Fitted maximal force following $ONNO^-$ administration. Steady state $ONOO^-$ concentrations of 300 nM resulted in contractile deficits; $ONOO^-$ as low as 50 nM impaired MM-CK activity (PCr/ATP developed tension). (C) Representative western blot of M-CK probed for extent of tyrosine nitration with 3NT antibody. $ONOO^-$ caused concentration-dependent increases in 3NT immunoreactivity of M-CK (migration of M-CK confirmed with antibody against M-CK). *$P<0.05$ vs. control; †$P<0.05$ vs ATP at 50 nM $ONOO^-$.

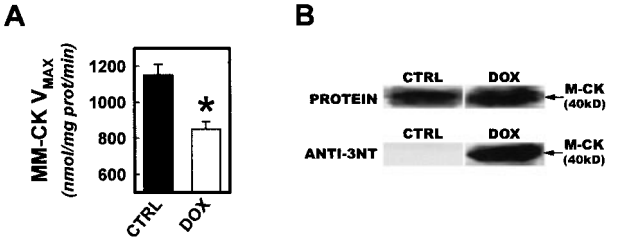

Figure 4 Nitration and inactivation of myofibrillar creatine kinase activity during DOX cardiotoxicity. (A) Left ventricular myofibrillar isolates were assessed for CK activity 5 days after treatment with DOX or vehicle control. (B) Myofibrillar isolates were probed for M-CK content and extent of protein nitration. Upper panels show representative protein bands for M-CK visualized with reversible protein stain. Lower panels are corresponding bands following immunoblotting analysis with anti-3NT antibody. In separate experiments, identity of M-CK band was confirmed using anti-M-CK antibody. *$P<0.05$.

lished event during this phenomenon (Singal, 1987; Hasinoff *et al*., 1998; Gille & Nohl, 1997; Papadopoulou *et al*., 1999). However, isolated myocyte experiments suggest that DOX-induced impairments in myofibrillar energetics may precede mitochondrial insults and errors in oxidative respiration (Sarvazyan *et al*., 1995). In preliminary immunohistochemical studies we observed increased protein nitration in cardiac tissues from DOX treated animals; high magnification light microscopy (oil immersion) showed that the nitration staining pattern paralleled the myofibrillar architecture. We then employed immunogold electron microscopy to evaluate intracellular prevalence of nitration events, with specific attention to mitochondrial versus myofibrillar compartments. We achieved sensitive and specific immunocytochemistry for 3NT, while maintaining morphological integrity sufficient to easily identify subcellular structures and organelles. The highly electron dense gold particles were easily quantifiable using current digital image analysis techniques, and over 8500 discrete particles were counted. We found that myocyte protein nitration was significantly elevated following DOX treatment, and found that 3NT density was equivalent in myofibrillar and mitochondrial spaces as a function of area. However, since myofibrillar area is roughly double that of mitochondrial area in cardiac myocytes (Zhou & Kang, 2000; Yates & Greaser, 1983), we found that total nitration load

(total myocyte 3NT density) was over 2 fold higher in cardiac myofibrils versus mitochondria in DOX treated mice. These results demonstrate that the cardiac myofibril is apparently a predominant target of nitration during DOX treatment and suggest that ONOO$^-$-myofibrillar interactions may be of particular importance during DOX cardiotoxicity. Interestingly, we have observed evidence of myofibrillar nitration and dysfunction in many other settings of chronic cardiac myocyte failure in several species, including humans (Mihm *et al*., 2001a, b). Thus, peroxynitrite formation and myofibrillar protein oxidation may be a universal and mechanistically important phenomenon. Our findings are highly consistent with recent studies implicating the myofilaments as central participants in contractile dysfunction during the initiation and progression of cardiac failure in general (Perez *et al*., 1999). Interestingly, we also observed detectable 3NT formation in both myofibrillar and mitochondrial spaces in CTRL cardiac tissue, consistent with the emerging view that tyrosine nitration may be a dynamic post-translational signaling event that, under certain conditions, may be a regulated and/or controlled modulator of protein structure and enzymatic function (Kamisaki *et al*., 1998; Piao *et al*., 2000).

In light of our observations implicating cardiac myofibrils as a predominant site of protein nitration during DOX cardiotoxicity, we assessed the functional consequences of myofibrillar exposure to ONOO$^-$ using isolated cardiac trabecular preparations. Skinned cardiac trabeculae provide an excellent model to study the contractile properties of the myofibrillar structure, particularly for the study of reactive species, since alternate oxidative targets (lipids, other organelles) are removed from the system through the skinning process (Mekhfi *et al*., 1996). We employed two different primary substrates for high energy phosphate production to fuel contractile activity: an ATP containing solution, which directly stimulates myosin ATPase to activate contraction, or a phosphocreatine containing solution, which elicits contraction only through the ATP producing capacity of MM-CK (Ventura-Clapier *et al*., 1987). We found that isolated myofibrillar contractile function was highly vulnerable to ONOO$^-$-mediated contractile impairment, at concentrations that are well within pathologically relevant concentrations of ONOO$^-$ *in vivo* (Beckman & Koppenol, 1996). While this may be related to direct impairment of the myosin ATPase, there are many other structural or contractile or regulatory proteins in the trabecula preparation that could be negatively affected under the conditions investigated. Interestingly, the most sensitive myofibrillar contractile component was MM-CK dependent contractile activity, as the ratio of PCr/ATP developed tension was impaired at 50 nM steady state concentrations of ONOO$^-$. Consistent with this finding, we found that MM-CK isolated from these trabecular preparations was nitrated by ONOO$^-$. At low concentrations of ONOO$^-$ (50 nM), MM-CK and myosin heavy chain were the only proteins demonstrating detectable protein nitration, suggesting that myofibrillar contractile activity, particularly myofibrillar ATP production capabilities, are highly vulnerable to ONOO$^-$.

Impairment in the CK system, and in the MM-CK isoform in particular, is an established event during clinical and experimental settings of decompensated cardiac failure, and may represent a unifying event in heart failure progression (Ventura-Clapier *et al*., 1994; Ingwall, 1998; Neubauer *et al*., 1997; Wallimann *et al*., 1998). Following our *in vitro* trabecular investigations, we evaluated MM-CK function in DOX treated mice; we observed an approximate 30% reduction in maximal MM-CK activity relative to vehicle controls with no change in MM-CK content by Western blotting. These kinetic results are consistent with irreversible oxidative injury and with other models of DOX cardiotoxicity both *in vitro* and *in vivo* (Deatley *et al*., 1999). Although the myofibrillar isoform of creatine kinase is responsible for ATP production at the site of contraction, an equally important functional role includes the suppression of ADP accumulation during contractile activity (Saks *et al*., 1975). Accumulation of ADP can lower the free energy of ATP hydrolysis and reduce the driving force for cardiac contraction. During normal contractile function, ADP concentrations remain below 10 μM, despite intracellular concentrations of ATP as high as 5–10 mM and resting ATP turnover rates on the order of 500 μM s^{-1} (Ingwall, 1997). The maintenance of such low ADP concentrations is largely due to the catalytic activity of MM-CK, by virtue of its location (bound to myofibrillar M-line coupled to ATPase) and extremely rapid reaction rate ($\sim$10 times ATPase V_{MAX}) (Ventura-Clapier *et al*., 1994). Elegant investigations (Tian *et al*., 1997) have demonstrated that experimental inhibition of the creatine kinase system resulting in $<$10% reductions in myocyte ATP concentrations can precipitate $>$2 fold increases in cellular ADP concentrations (Tian *et al*., 1997). Elevated ADP concentrations result in significant elevations in LVEDP and decreased LVSP in isolated rat heart preparations. Therefore, the seemingly modest (30%) reduction in MM-CK V_{MAX} observed during DOX cardiotoxicity may have mild effects on ATP production activities, but more dramatic effects on ADP concentrations, contributing to energetic dysregulation and resultant contractile deficit. Measurement of subcellular ADP pools is not yet technically feasible with current methods, but could add important insight in this setting.

In summary, DOX caused significant LV dysfunction in mice similar to clinically observed events. Since ONOO$^-$-mediated injury may be an important mechanism of DOX-induced cardiotoxicity (as well as other forms of cardiac decompensation), we used this model to investigate the relative sub-cellular distribution of protein nitration events, and found that the cardiac myofibril is a primary site of protein nitration during DOX cardiotoxicity. Mechanistic investigations revealed that this contractile structure is highly sensitive to ONOO$^-$-mediated injury, particularly the myofibrillar isoform of creatine kinase. *In vivo* determinations were consistent with these results, demonstrating significant nitration and inactivation of MM-CK during DOX cardiotoxicity. These findings suggest that ONOO$^-$-myofibrillar interactions, particularly those involving myofibrillar energetics and MM-CK, may mediate some aspects of DOX cardiotoxicity *in vivo* and that strategies to affect these interactions may have therapeutic value.

We appreciate the expert technical assistance of Ms Kathy Wolken, MS, The Ohio State University Microscopy Facility. This work was supported in part by grants from the National Institutes of Health (HL59791, DK55053, HL63067)

References

BECKMAN, J.S. & KOPPENOL, W. (1996). Nitric oxide, superoxide, and peroxynitrite: the good, the bad, and the ugly. *Am. J. Physiol., 271,* C1424–1437

BLUM, R.H. & CARTER, S.K. (1974). Adriamycin. A new anticancer drug with significant clinical activity. *Ann. Intern. Med.,* **80,** 249–259

CROUSER, E.D., JULIAN, M.W., WEINSTEIN, D.M., FAHY, R.J. & BAUER, J.A. (2000). Endotoxin-induced ileal mucosal injury and nitric oxide dysregulation are temporally dissociated. *Am. J. Resp. Crit. Care. Med.,* **161,** 1705–1712.

DEATLEY, S.M., AKSENOV, M.Y., AKSENOVA, M.V., JORDAN, B., CARNEY, J.M. & BUTTERFIELD, D.A. (1999). Adriamycin-induced changes of creatine kinase activity *in vivo* and in cardiomyocyte culture. *Toxicology,* **134,** 51–62.

DOROSHOW, J.H., LOCKER, G.Y.& MYERS, C.E. (1979). Experimental animal models of adriamycin cardiotoxicity. *Cancer Treat. Rep.,* **63,** 855–860

FELKER, G.M., THOMPSON, R.E., HARE, J.M., HRUBAN, R.H., CLEMETSON, D.E., HOWARD, D.L., BAUGHMAN, K.L. & KASPER, E.K. (2000). Underlying causes and long-term survival in patients with initially unexplained cardiomyopathy. *New Engl. J. Med.,* **342,** 1077–1084.

GILLE, L. & NOHL, H. (1997). Analyses of the molecular mechanism of adriamycin-induced cardiomyopathy. *Free Rad. Biol. Med.,* **23,** 775–782.

HASINOFF, B.B., HELLMANN, K., HERMAN, E.H. & FERRANS, V.J. (1998). Chemical, biological and clinical aspects of dexrazoxane and other bisdioxopiperazines. *Curr. Med. Chem.,* **5,** 1–28.

HORTOBAGYI, G.N. (1997). Anthracyclines in the treatment of cancer. An overview. *Drugs,* **54,** 1–7

INGWALL, J.S. (1997). In: *Heart Failure: Scientific Principles and Clinical Practice*. New York, NY: Churchill-Livingstone.

INGWALL, J.S. (1998). Creatine kinase knockout mice − what is the phenotype: heart. *MAGMA* **6,** 120–121.

ISCHIROPOULOS, H. (1998). Biological tyrosine nitration: a pathophysiological function of nitric oxide and reactive oxygen species. *Arch. Biochem. Biophys.,* **356,** 1–11.

KAMISAKI, Y., WADA, K., BIAN, K., BALABANLI, B., DAVIS, K., MARTIN, E., BEHBOD, F., LEE, Y.C. & MURAD, F. (1998). An activity in rat tissues that modifies nitrotyrosine-containing proteins. *Proc. Natl. Acad. Sci. U.S.A.,* **95,** 11584–11589.

KOOY, N., LEWIS, S., ROYALL, J., YE, Y., KELLY, D & BECKMAN, J. (1997). Extensive tyrosine nitration in human myocardial inflammation. *Crit. Care Med.,* **25,** 812–819.

KWOK, J.C. & RICHARDSON, D.R. (2000). The cardioprotective effect of the iron chelator dexrazoxane (ICRF-187) on anthracycline-mediated cardiotoxicity. *Redox. Rep.,* **5,** 317–324.

LIPSHULTZ, S.E. & GRENIER, M.A. (1999). Doxorubicin-induced cardiomyopathy. *New Engl. J. Med.,* **340,** 654.

MEKHFI, H., VEKSLER, V., MATEO, P., MAUPOIL, V., ROCHETTE, L & VENTURA-CLAPIER, R. (1996). Creatine kinase is the main target of reactive oxygen species in cardiac myofibrils. *Circ. Res.,* **78,** 1016–1027.

MIHM, M.J., COYLE, C., SCHANBACHER, B.L., WEINSTEIN, D.M. & BAUER, J.A. (2001a). Peroxynitrite induced nitration and inactivation of myofibrillar creatine kinase in experimental heart failure. *Cardiovasc. Res.,* **49,** 798–807.

MIHM, M.J., YU, F., CARNES, C.A., REISER, P.J., MCCARTHY, P.M. VAN WAGONER, D.R. & BAUER, J.A. (2001b). Impaired myofibrillar energetics and oxidative injury during human atrial fibrillation. *Circulation,* **104,** 174–180.

MIHM, M.J., COYLE, C.M., JING, L. & BAUER, J.A. (1999). Vascular peroxynitrite formation during organic nitrate tolerance. *J. Pharmacol. Exp. Ther.,* **291,** 194–198.

MUGGIA, F.M. & SPEYER, J.L. (1999). Doxorubicin-induced cardiomyopathy. *New Engl. J. Med.,* **340,** 654.

NEUBAUER, S., HORN, M., CRAMER, M., HARRE, K., NEWELL, J.B., PETERS, W., PABST, T., ERTL, G., HAHN, D., INGWALL, J.S. & KOCHSIEK, K. (1997). Myocardial phosphocreatine-to-ATP ratio is a predictor of mortality in patients with dilated cardiomyopathy. *Circulation,* **96,** 2190–2196.

PAPADOPOULOU, L.C., THEOPHILIDIS, G., THOMOPOULOS, G.N. & TSIFTSOGLOU, A.S. (1999). Structural and functional impairment of mitochondria in adriamycin-induced cardiomyopathy in mice: suppression of cytochrome c oxidase II gene expression. *Biochem. Pharmacol.,* **57,** 481–489.

PEREZ, N.G., HASHIMOTO, K., MCCUNE, S., ALTSCHULD, R.A. & MARBAN, E. (1999). Origin of contractile dysfunction in heart failure: calcium cycling versus myofilaments. *Circulation,* **99,** 1077–1083.

PIAO, S., WATTANAPITAYAKUL, S.K., MIHM, M.J. & BAUER, J.A. (2000). Angiotensin induced peroxynitrite formation and selective enzymatic modification of nitrated protein in endothelial cells. *Circulation,* **102,** II-245 (Abstract).

RADI, R., BECKMAN, J., BUSH, K. & FREEMAN, B. (1991). Peroxynitrite-Induced membrane lipid peroxidation: the cytotoxic potential of superoxide and peroxynitrite. *Arch. Biochem. Biophys.,* **288,** 481–487.

SAKS, V., CHERNOUSOVA, G., GUKOVSKY, E., SMIRNOV, V. & CHAZOV, E. (1975). Studies of energy transport in heart cells. *Eur. J. Biochem.,* **57,** 273.

SAMPSON, J., ROSEN, H. & BECKMAN, J. (1996). Peroxynitrite-dependent tyrosine nitration catalyzed by superoxide dismutase, myeloperoxidase, and horseradish peroxidase. *Method. Enzymol.,* **269,** 210–218.

SARVAZYAN, N.A., ASKARI, A. & HUANG, W.H. (1995). Effects of doxorubicin on cardiomyocytes with reduced level of superoxide dismutase. *Life Sci.,* **57,** 1003–1010.

SINGAL, P.K. (1987). Subcellular effects of Adriamycin in the heart: a concise review. *J. Mol. Cell. Cardiol.,* **19,** 817–828.

SWAIN, S.M. (1999). Doxorubicin-induced cardiomyopathy. *New Engl. J. Med.,* **340,** 654.

TIAN, R., CHRISTE, M.E., SPINDLER, M., HOPKINS, J.C.A., HALOW, J.M., CAMACHO, S.A. & INGWALL, J.S. (1997). Role of MgADP in the development of diastolic dysfunction in the intact beating rat. *Heart J. Clin. Invest.,* **99,** 745–751.

VAN DER VIJGH, W.J., MAESSEN, P.A. & PINEDO, H.M. (1990). Comparative metabolism and pharmacokinetics of doxorubicin and 4′-epidoxorubicin in plasma, heart and tumor of tumor-bearing mice. *Cancer Chemother. Pharmacol.,* **26,** 9–12.

VENTURA-CLAPIER, R., SAKS, V.A., VASSORT, G., LAUER, C. & ELIZAROVA, G.V. (1987). Reversible MM-creatine kinase binding to cardiac myofibrils. *Am. J. Physiol.,* **253,** C444–C455.

VENTURA-CLAPIER, R., VEKSLER, V. & HOERTER, J. (1994). Myofibrillar creatine kinase and cardiac contraction. *Mol. Cell. Biochem.,* **133/134,** 125–144.

WALLIMANN. T., DOLDER, M., SCHLATTNER, U., EDER, M., HORNEMANN, T., KRAFT, T. & STOLZ, M. (1998). Creatine kinase: an enzyme with a central role in cellular energy metabolism. *MAGMA,* **6,** 116–119.

WATTANAPERMPOOL, J. & REISER, P.J. (1999). Differential effects of ovariectomy on calcium activation of cardiac and soleus myofilaments. *Am. J. Physiol.,* **277,** H467–H473.

WEINSTEIN, D.M., MIHM, M.J. & BAUER, J.A. (2000). Cardiac peroxynitrite formation and left ventricular dysfunction following doxorubicin treatment in mice. *J. Pharmacol. Exp. Ther.,* **294,** 396–401.

YATES, L.D. & GREASER, M.L. (1983). Quantitative determination of myosin and actin in rabbit skeletal muscle. *J. Mol. Biol.,* **168,** 123–141.

YEN, H.C., OBERLEY, T.D., VICHITBANDHA, S., HO, Y.S. & ST CLAIR, D.K. (1996). The protective role of manganese superoxide dismutase against adriamycin-induced acute cardiac toxicity in transgenic mice. *J. Clin. Invest.,* **98,** 1253–1260.

ZHOU, Z. & KANG, Y.J. (2000). Immunocytochemical localization of metallothionein and its relation to doxorubicin toxicity in transgenic mouse heart. *Am. J. Pathol.,* **56,** 1653–1662.

(Received June 15, 2001
Revised August 8, 2001
Accepted November 12, 2001)